International Journal of Nanomedicine

Dovepress
open access to scientific and medical research

Open Access Full Text Article

ORIGINAL RESEARCH

Chitosan/Hyaluronic Acid/MicroRNA-21 Nanoparticle-Coated Smooth Titanium Surfaces Promote the Functionality of Human Gingival Fibroblasts

Zhongshan Wang[1,*], Guangsheng Wu[2,*], Zhujun Yang[3], Xuejian Li[1], Zhihong Feng[1], Yimin Zhao[1]

[1]State Key Laboratory of Military Stomatology & National Clinical Research Center for Oral Diseases & Shaanxi Key Laboratory of Oral Diseases, Department of Prosthodontics, School of Stomatology, Fourth Military Medical University, Xi'an, People's Republic of China; [2]Qingdao Special Servicemen Recuperation Center of PLA Navy, Qingdao, People's Republic of China; [3]Xi'an Central Hospital Affiliated to Xi'an Jiaotong University, Xi'an, Shaanxi, 710003, People's Republic of China

*These authors contributed equally to this work

Correspondence: Zhongshan Wang; Yimin Zhao, State Key Laboratory of Military Stomatology & National Clinical Research Center for Oral Diseases & Shaanxi Key Laboratory of Oral Diseases, Department of Prosthodontics, School of Stomatology, Fourth Military Medical University, Xi'an, 710032, People's Republic of China, Tel/Fax +86-29-84776128, Email wzs_fmmu@163.com; zhaoymdentist@163.com

Purpose: Forming a compact biological seal between the gingiva and the implant interface around the percutaneous parts of an implant is one of the key issues in preventing peri-implantitis.

Methods: In this study, since microRNA-21 (miR-21) has been approved to promote fibroblast proliferation and collagen formation in skin fibrosis, we prepared miR-21-loaded chitosan (CS)/tripolyphosphate (TPP)/hyaluronic acid (HA) nanoparticles (CTH NPs) and cross-linked them to smooth Ti surfaces with 0.2% gel solution for reverse transfection, after which isolated human gingival fibroblasts were cultured on the miR-21-functionalized Ti substrates.

Results: An optimal CS:TPP:HA ratio (1:0.15:0.1) and N/P ratio (20:1) were chosen to produce appropriate nanoparticles. Finally, the CTH/miR-21 nanoparticle-coated smooth Ti surfaces demonstrated increased fibroblast adhesion, proliferation and expression of extracellular matrix-related genes along with similar cytotoxicity and cell spreading on the miR-21-functionalized Ti surface and the unmodified smooth Ti surface.

Conclusion: The chitosan-based nanoparticles might be an efficient nonviral miRNA vector to form a stable biological seal in percutaneous areas of Ti for clinical use.

Keywords: microRNA, chitosan, hyaluronic acid, nanoparticle, percutaneous implant

Introduction

Titanium has been widely adopted as a temporary or permanent percutaneous implant to support and stabilize prostheses due to its high biocompatibility, biochemical stability, and mechanical strength.[1] However, in contrast to the stable osseointegration of the intraosseous parts of implants, the percutaneous areas always lack tight biointegration, resulting in multiple predictable failure patterns, including mechanical avulsion, bacterial attacks, and epithelial downgrowth, which impairs the long-term success of implants.[2,3] As the primary cells of skin tissues, dermal fibroblasts play essential roles in skin-implant integration and are recruited and activated once a percutaneous wound is formed.[2,3] Fibroblasts proliferate and secrete essential components of the extracellular matrix (ECM), including type I and III collagen, to provide structural support for tissue healing.[4] In the later remodelling stage, fibroblasts differentiate into myofibroblasts characterized by alpha-smooth muscle action (α-SMA),[5,6] and myofibroblasts can produce continual tension to promote wound contraction. Therefore, it is beneficial to facilitate fibroblast adhesion, proliferation, and production of ECM for the formation of early tight skin-implant biointegration[2] and strengthen the long-term stability of percutaneous implants.

Received: 18 May 2022
Accepted: 25 August 2022
Published: 1 September 2022

To achieve a stale biological seal in the early stage, cells need to win the "surface race" with microorganisms,[7] which means fibroblasts must attach to the Ti surface faster than bacteria, forming the cellular layer immediately attached the Ti surface and making the percutaneous areas of implants less available for bacterial attachment. However, if bacteria win the "race", biofilms will be established quickly and become less susceptible to removal.[8] Highly polished Ti surfaces have been widely used at percutaneous segments due to decreased bacterial aggregation and improved cellular adhesion and spread compared to rough titanium surfaces.[2] However, such an unmodified smooth surface still suffers from marsupialization with epithelial downgrowth and bacterial attacks. Previous researchers made a series of surface coatings on β-FeOOH/Fe-TiO2 heterojunctions,[9] Si-substituted hydroxyapatite (Si-HA) nanorods,[10] fibrinogen mediated by the macromolecule polydopamine, and so on;[7,11] others made antibacterial agent coatings[12] or altered the topography of implants.[13] However, most of the approaches still made the Ti surfaces rougher and more complicated, showing limited success in enhancing cellular amplification and deterring bacterial invasion. Hence, more effective measures are necessary to solve this problem.

MicroRNAs (miRNAs) consisting of 18–22 nucleotides function as gene regulators by binding primarily to the 3' untranslated region (UTR) of mRNAs to accelerate mRNA degradation or inhibit mRNA translation.[14] As endogenous noncoding RNAs, miRNAs participate in different biological behaviours, such as migration, differentiation, and ECM synthesis.[15] In recent years, researchers have demonstrated that overexpression of miRNA-21 (miR-21) has a critical role in skin fibrosis,[16,17] such as hypertrophic scars, keloids, and scleroderma. miR-21 contributes to increased cell proliferation, decreased apoptosis, and rapid extracellular matrix (ECM) deposition in skin fibrosis,[18,19] which suggests that delivering more miR-21 to Ti surfaces may promote gingival fibroblast proliferation and ECM production to help form a stable biological seal in the early stage.

Vectors are usually necessary to protect and deliver miRNAs intracellularly. In previous studies, various viral vectors have been widely designed as efficient carriers for gene therapy. However, nonviral gene-delivery vectors are a viable alternative for clinical application because of safety concerns, favourable biocompatibility and decreased host immune response.[20] As a natural polysaccharide, chitosan (CS) has been widely employed as a controlled-release drug-delivery carrier due to various favourable features, including excellent biocompatibility, fast degradation and high gene transfection efficiency.[21,22] Its positive charges contribute to nanoscale complex formation with negatively charged siRNAs or miRNAs, which can also be absorbed to negatively charged cell surfaces with phosphate groups.[22] HA is a natural anionic polysaccharide in mammals that can also effectively bind the cell adhesion protein CD44, which is expressed in normal human fibroblasts, MSCs, cancerous cells and others.[23] In addition, tripolyphosphate (TPP) plays a role in crosslinking to modify the morphology of nanoparticles.[24] To date, little work has addressed the use of chitosan/tripolyphosphate/hyaluronic acid nanoparticles (CTH NPs) for the delivery of miR-21 to dermal gingival fibroblasts to promote extracellular matrix deposition.

In this design, CTH/miR-21 NPs were prepared and characterized in terms of particle size, surface morphology, zeta potential and gel retardation. Then, the CTH/miR-21 NPs were previously cross-linked onto smooth Ti substrates with 0.2% gel solution. Afterwards, human gingival fibroblasts were seeded on the functionalized Ti surface. Furthermore, we evaluated the transfection efficiency, cytotoxicity, adhesion, and ECM-related gene expression in fibroblasts. We expect this novel design to enable an enhanced biological seal at percutaneous areas of implants for clinical use.

Materials and Methods

Materials

Chitosan (CS) of 100 kDa with a deacetylation degree of 90%was purchased from Jinke Co., Ltd. (Zhejiang, China). Tripolyphosphate (TPP) and gelatine powder (type A) were obtained from Sigma (St. Louis, USA). Hyaluronic acid (HA) of 10 kDa was purchased from C.P. Freda Pharmaceuticals Ltd. (Shangdong, China) The hsa-miR-21 mimics (5'-uagcuuaucagacugauguugadTdT-3'; 5'-ucaacaucagucugauaagcuadTdT-3') were obtained from Shanghai GenePharma Co., Ltd. (Shanghai, China). Titanium substrates 1.0 mm thick and 14 mm in diameter (99.9%) were fabricated by the Northwest Institute for Nonferrous Metal Research (Xi'an, China). Collagenase type I, dispase and glutamine were purchased from Sigma (St. Louis, USA). Foetal bovine serum and α-MEM were provided by HyClone (MA, USA). The

LDH cytotoxicity assay kit and CCK-8 were produced by Beyotime (Jiangsu, China). Real-time PCR primers were provided by Shanghai Sangon (Shanghai, China).

Preparation of CTH/miR-21 Nanoparticles

CTH/miR-21 nanoparticles were fabricated based on the ionotropic gelation technique used in our previous study.[21] Chitosan (1%, w/v) was dissolved in 0.1 M acetic acid solution at pH 5.5. TPP (1 mg/mL) and HA (1 mg/mL) were mixed in deionized water at pH 5.5 and filtered using 0.22 μm membranes. Mixtures with different CS: TPP: HA ratios were chosen to produce nanoparticles. CTH NPs were formed as soon as the TPP/HA solution was added dropwise to a fixed volume of CS solution. CTH/miR-21 NPs were fabricated by pipetting 50 μM miR-21 gently into the required volume of the CTH NPs gently to form complexes, followed by rapid vortex mixing for 3–5 seconds and allowing the mixture to stand at room temperature for 60 minutes to complete development. The molar ratio of the positive CS amino group versus the negative miRNA phosphate group was used to describe the N/P ratio.

Characterization of CTH/miR-21 NPs

The morphology of the NPs was observed using a transmission electron microscope (TEM, FEI Company, USA). The zeta potential and diameter of CTH/miR-21 NPs were determined by dynamic light scattering with a Nano ZS90 (Malvern, UK). For gel retardation analysis, the naked miR-21 and CTH/miR-21 NPs with various N/P ratios of 1:1, 5:1, 10:1, 15:1, 20:1 and 25:1 were loaded onto a 2% agarose gel containing ethidium bromide in Tris–borate EDTA buffer (pH 8.0). The gel retardation was determined by gel electrophoresis at 110 V for 20 min and then photographed using an image-acquisition system (UVP GDS-8000, CA, USA).

Specimen Fabrication and Surface Characterization

Titanium foils were polished sequentially using SiC sandpapers from 400 to 2000 grits and then ultrasonically cleaned for 10 minutes with acetone, ethanol, and deionized water sequentially. Then, the titanium foils were air-dried and irradiated by cobalt 60. A 0.2% gelatine (w/v) solution was used to attach the CTH/miR-21 NPs to titanium foils for reverse transfection.[20] In brief, the gelatine was dissolved in distilled water in a 60°C water bath. After high-temperature, high-pressure disinfection, the solution was cooled and stored at 4°C. Afterwards, 50 μM miR-21 solution was mixed with a required volume of blank CTH NP solution to produce CTH/miR-21 NP solution with an N/P ratio of 20:1. For cross-linking of CTH/miR-21 NPs, 50 μL gelatine solution was mixed gently with different volumes of CTH/miR-21 NP solutions containing 150, 300 and 450 pmol miR-21. The mixtures were pipetted onto the Ti substrates using 200 μL tips, dispersed as evenly as possible, and then freeze-dried.

To characterize the surface morphology, the previous gel or CTH/miR-21 NP-coated Ti substrates were fixed using glutaraldehyde and dehydrated with graded ethanol concentrations. After spraying with gold, the samples were photographed using FE-SEM (Hitachi S-4800, Tokyo, Japan).

To determine the distribution of CTH NPs and miR-21 after cross-linking, FITC-labelled chitosan and Cy3-labelled miR-21 were applied to prepare CTH/miR-21 NPs, which were coated onto Ti substrates as above. The FITC and Cy3 fluorescence signals were imaged using fluorescence microscopy (Olympus, Tokyo, Japan).

Contact angle measurements were determined by a sessile drop method using distilled water. The drop shapes on different samples were photographed, and the contact angles were measured using DSA1 software (KRUSS GmbH).

Isolation and Characterization of Human Dermal Fibroblasts

Primary fibroblasts were acquired using a previous method.[2] Gingival tissue was resected when extracting impacted third molars (22–28 years old, n = 3) with IRB approval from the Stomatological Hospital of FMMU and written informed consent. The gingival tissues were cut into tiny pieces and then digested using 1% dispase and 1% collagenase type I dissolved in 5 mL α-MEM at 37°C for 40 min. Then, the isolated cell types were centrifuged and incubated in culture medium containing α-MEM supplemented with 10% foetal bovine serum in a cell culture incubator with 5% CO_2 at 37°C. The medium was refreshed every 3 days, and fibroblasts at passages 2–5 were used in the study.

For the colony-forming unit-fibroblast (CFU-F) assay, fibroblasts at passage two were seeded at a density of 1×10^3 cells per ten-cm dish. After 10 days, the cells were fixed and stained with 0.1% crystal violet. Cell colonies were defined as aggregates of 50 or more cells viewed under the microscope.

Cytotoxicity and Cell Transfection

The lactate dehydrogenase (LDH) activity of the culture medium was determined spectrophotometrically. Briefly, fibroblasts were cultured in the medium for 24 h at 150, 300 and 450 pmol miR-21/specimen concentrations, and then the supernatant of each sample was analysed for LDH activity (n=3).

A flow cytometer (BD Biosciences, USA) was used to measure the transfection efficiency of CTH/miR-21 NPs. Briefly, Cy3-labelled miR-21 was applied to prepare fluorescence-labelled CTH/miR-21 NPs cross-linked onto Ti substrates as above. Then, fibroblasts (P3) were seeded at a density of 2×10^5 cells/specimen. After 24 h, fibroblasts were digested, washed, and then fixed. The Cy3 fluorescence emitted by fibroblasts because of phagocytosis was detected using a flow cytometer, while the negative control group was subjected to the same process (n=3).

The fluorescence of internalized NPs was tracked by fluorescence microscopy (Olympus, Tokyo, Japan). Briefly, fluorescently labelled CTH/miR-21 NPs were applied, and fibroblasts were transfected with the optimal volume of miR-21 at a concentration of 300 pmol/specimen. After 1, 5, and 10 days, the cells were immediately fixed, and their nuclei were stained with DAPI (Sigma, USA) and washed twice in PBS. Afterwards, the fluorescence signals were traced under microscopy.

Cell Adhesion and Cell/Bacteria Proliferation Assay

Fibroblasts were seeded onto Ti substrates placed in 24-well culture plates in serum-free media at a density of 5×10^4 cells/well. A concentration of 300 pmol/specimen miR-21 was used for reverse transfection. After incubating for 0.25, 0.5, 1 and 2 hours, the attached fibroblasts were washed twice in PBS, fixed, and stained with DAPI. Then, the adherent cell numbers were counted in five random areas (50x, 2.60 mm × 1.94 mm per area) of each specimen with a fluorescence microscope (Olympus, Tokyo, Japan) (n=6).

Fibroblasts were seeded on the naked and functionalized Ti specimens at a density of 2×10^3 cells/specimen in 24-well culture plates. A concentration of 300 pmol/specimen miR-21 was used for reverse transfection. After 1, 3, and 5 days, the CCK-8 kit was used to assay the cell proliferation. Briefly, the substrates were rinsed twice. The CCK-8 reagent was first mixed with fresh culture medium according to the required proportion, and then 1 mL was added to each specimen, followed by incubation for 2 hours at 37°C. Afterwards, an aliquot (100 μL) of medium was transferred into a 96-well plate and assessed by a spectrophotometer (Bio-Tek) at 450 nm. The assessments were repeated on six different substrates for each sample.

20 μL of Porphyromonas gingivalis strain preservation solution was inoculated in 2mL BHI blood broth medium (3.7g BHI broth dry powder was dissolved in 100mL distilled water, autoclaved at 121 °C for 15 minutes and cooled to 50 °C. Sterile defibrinated sheep blood and hemin-vitamin K were added at the concentrations of 1:10 and 1:100 respectively, and then mixed evenly by shaking.), and put into an anaerobic culture bag, followed by incubation at 37°C for 48h. The concentration of the bacterial solution was adjusted to the absorbance of 0.5 at 600nm, and then an aliquot (1mL) of bacterial solution was added to each specimen in an anaerobic culture bag, followed by incubation at 37°C for 12, 24, 36, 48, and 60 hours, respectively. Afterwards, the bacterial liquid was recovered from each sample, and the absorbance was detected at 600nm. The assessments were repeated on three different substrates for each sample.

Cell Morphology

Cells (P3) were seeded onto noncoated and CTH/miR-21-coated smooth Ti substrates at a density of 1×10^5 cells/specimen in 24-well plates. A concentration of 300 pmol/specimen miR-21 was used for reverse transfection. At five days post-transfection, the cells cultured on substrates were fixed and observed by FE-SEM.

ECM-Related Gene Expression

The expression levels of ECM-related genes, including COL1A1, COL3A1 and α-SMA, were evaluated using real-time PCR. Briefly, fibroblasts were transferred onto each specimen at a density of 5×10^4 cells/well in 24-well plates and incubated for 3 or 7

days. Then, the total nucleic acid was harvested using the TRIzol reagent (Takara, Otsu, Japan), and an equivalent amount of RNA from each specimen was reverse-transcribed into complementary DNA (cDNA). The forward/reverse primer sequences for the targeted genes were as follows: COL1A1: 5′-GAGGGCCAAGACGAAGACATC-3′, 5′-CAGATCACGT CATCGCACAAC-3′; COL3A1: 5′-GGAGCTGGCTACTTCTCGC-3′, 5′-GGGAACATCCTCCTTCAACAG-3′; α -SMA: 5′-AAAAGACAGCTACGTGGGTGA′-3′, 5′-GCCATGTTCTATCGGGTACTTC-3′. The reaction products were quantified by a CFX Connect™ Real-Time PCR Detection System (Bio–Rad CA, USA). The relative expression levels of the target genes were normalized to the expression of the housekeeping gene.

Statistical Analyses

The results were collected and analysed with SPSS 18.0 software (SPSS, IBM, NY, USA) and expressed as the mean ± standard deviation. The significance level was determined using a two-way analysis of variance and Student–Newman–Keuls q-tests or Student's *t* test. Differences were considered statistically significant with a p value of < 0.05.

Results

Characterization of CTH/miR-21 Nanoparticles

CTH nanoparticles were produced via ionic gelation between positively charged CS and negatively charged TPP and HA. Afterwards, miR-21 was incorporated into CTH NPs by electrostatic attraction to form CTH/miR-21 complexes. The surface morphologies of CTH/miR-21 NPs were photographed by TEM (Figure 1A) and SEM (Figure 2E and F), and the results showed that the CTH/miR-21 NPs were finely dispersed and displayed even spherical shapes in the visual field. The selected CTH/miR-21 NPs in this study presented an average diameter of 181.3 ± 11.45 nm and adequate zeta potential of 34.2 ± 5.3 mV at a 1:0.15:0.1 ratio of CS:TPP:HA and a 20:1 ratio of N/P (Figure 1C and D).

The binding capacity of CTH nanoparticles with miR-21 was confirmed by the gel retardation assay. Various N/P ratios of the CTH miR-21 NPs at 1:1, 5:1, 10:1, 15:1, 20:1 and 25:1 were prepared. The results demonstrated that miR-21 remained completely within the agarose gel loading well when the N/P ratio greatly exceeded 15:1, suggesting that the incorporation of miR-21 with CTH NPs was determined by the N/P ratio (Figure 1B).

Characterization of CTH/miR-21 NP-Coated Ti Surfaces

In this section, we used a 0.2% gel solution to cross-link the NPs onto smooth Ti substrates for reverse transfection. The SEM micrographs (Figure 2A and B) show that the highly polished Ti substrates were relatively smooth with sporadic minor grooves and pits; the gelatine-coated Ti substrates displayed highly aligned and ordered gelatine protein layers (Figure 2C and D); and the CTH/miR-21 NP-coated Ti substrates exhibited a uniform and sleek coating of CTH/miR-21 NPs, which were embedded tightly in gelatine proteins and were evenly dispersed to form a monolayer (Figure 2E and F).

To further determine the locations and distributions of CS/HA/miR-21 NPs after coating on the Ti substrates, Cy3-labelled miR-21 s and FITC-labelled CS were adopted to prepare NPs. As Figure 3A shows, both Cy3-labelled miR-21 and FITC-labelled CS were distributed uniformly. The overlapped fluorescence implied that the miR-21 molecules were still retained in CS/HA NPs after the coating of CTH/miR-21 NPs onto substrates.

Both the gel-coated Ti substrates and CTH/miR-21 NP-coated Ti substrates exhibited increased surface energy in the contact angle assay. The results in Figure 3B showed that the water contact angle of smooth Ti substrates was approximately 83.2°±3.4°, the gel-coated substrates displayed higher hydrophilicity with a smaller contact angle of 41.5°±2.8°, and the CTH/miR-21 NP-coated substrates showed similar hydrophilicity with a contact angle of 43.7°±2.5°. Different water contact angles on different samples implied that the surface chemistry changed significantly.

Cytotoxicity and Transfection Efficiency Assays of CTH/miR-21 NP-Coated Ti Surfaces

As shown in Figure 4A, the primary human gingival fibroblasts presented a long spindle-shaped morphology. The proliferative potential of fibroblasts was measured by cloning ability (Figure 4B). The results demonstrated an excellent colony formation rate after ten days of culture.

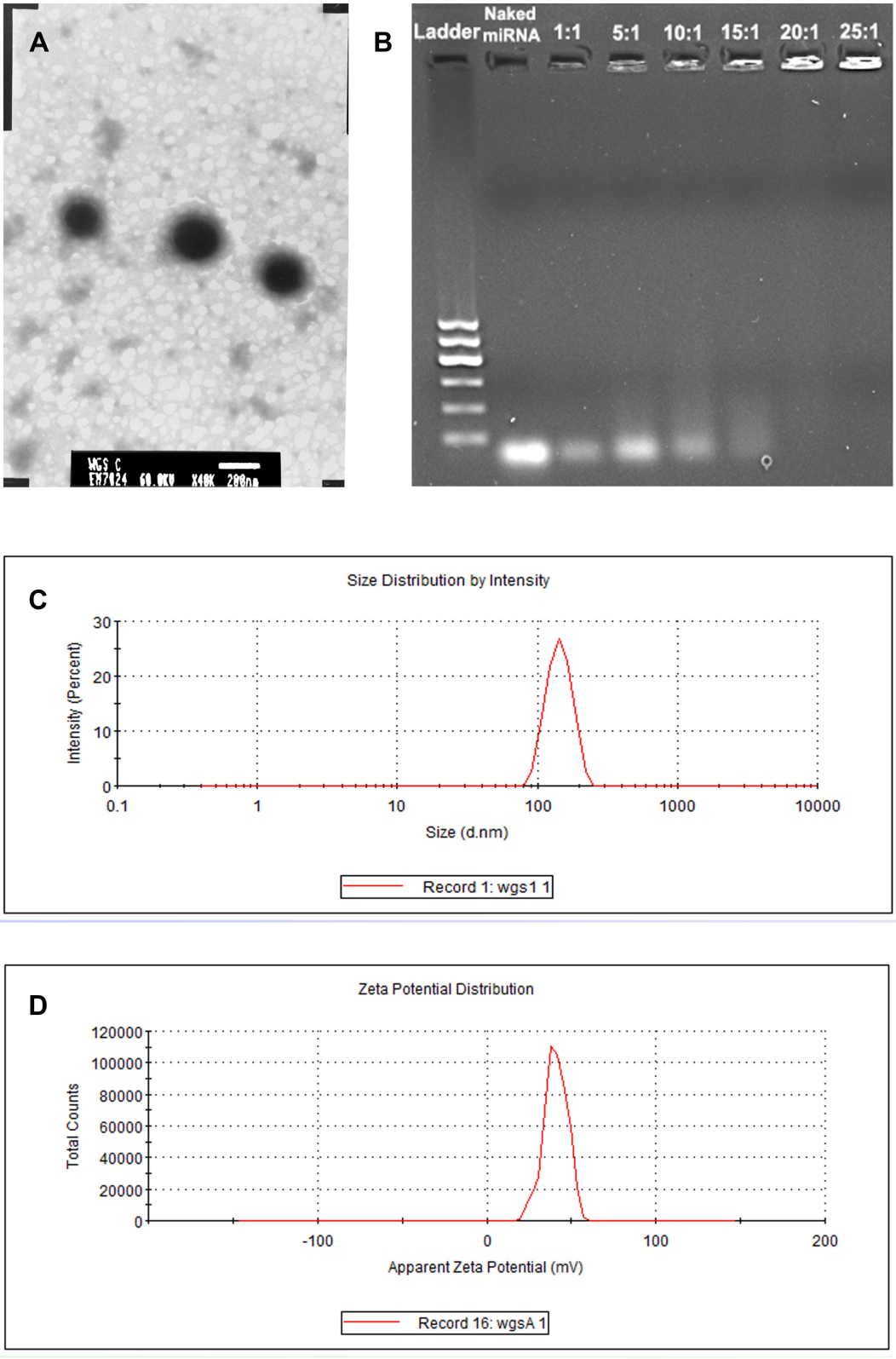

Figure 1 Characterization of CTH/miR-21 NPs.

Notes: (**A**) TEM images of CTH/miR-21 NPs with a scale bar of 200 nm. (**B**) Gel retardation analysis of CTH/miR-21 NPs; Lane 1, ladder; Lane 2, naked miR-21; Lanes 3–8, CTH/miR-21 NPs fabricated at N/P ratios of 1:1, 5:1, 10:1, 15:1, 20:1 and 25:1. (**C**) The size distribution of the CTH/miR-21 NPs prepared from an optimal mixture with CS: TPP: HA at a volume ratio of 1:0.15:0.1. (**D**) The zeta potential distribution of the CTH/miR-21 NPs.

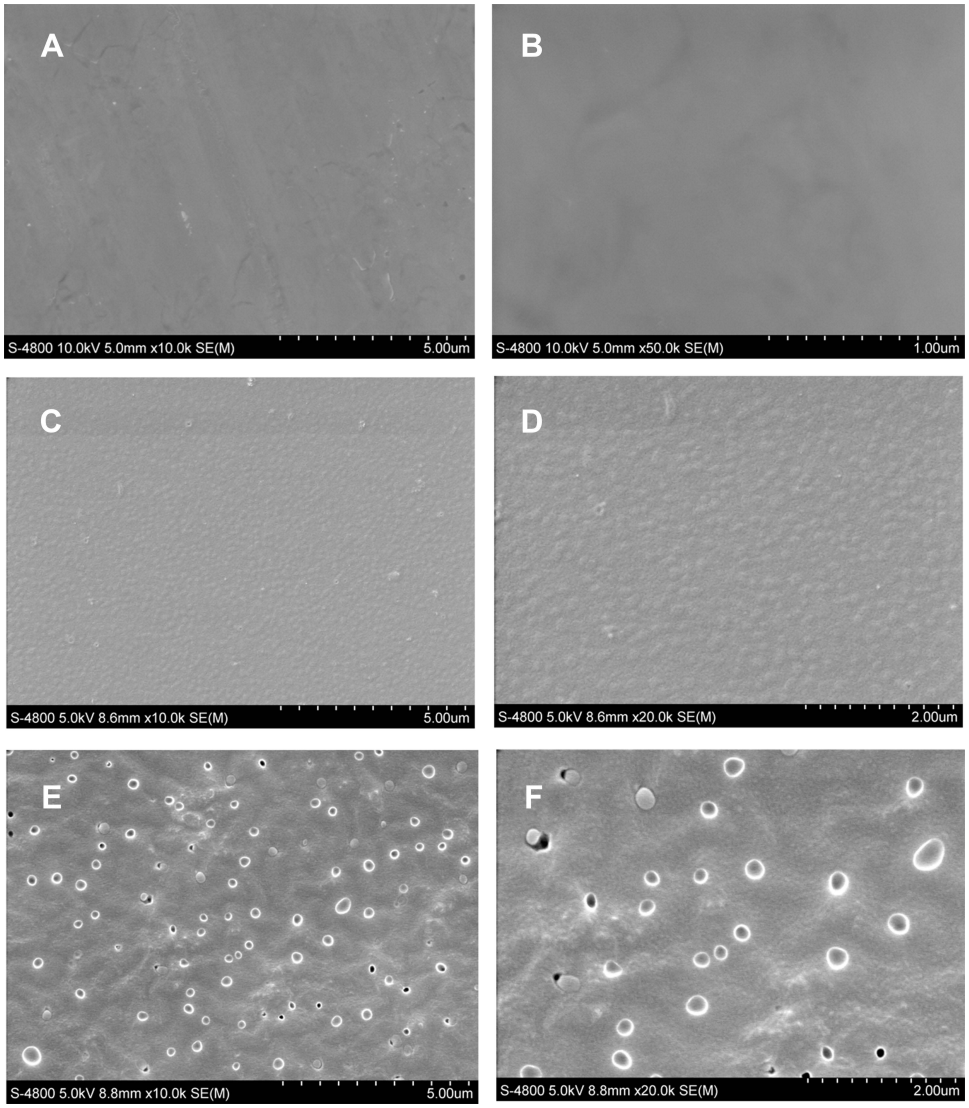

Figure 2 SEM images of unmodified and coated Ti substrates.
Notes: (**A** and **B**) SEM image of smooth Ti substrates with increasing magnification. (**C** and **D**) SEM image of 0.2% gel solution-coated Ti substrates with increasing magnification. (**E** and **F**) SEM image of CTH/miR-21 NP-coated Ti substrates with increasing magnification.

The activity of LDH was used as an indicator of the cytotoxicity of different substrates after 24 h of transfection, as depicted in Figure 4C. The results indicated that neither the Ti substrate coated with vacant CTH NPs nor that coated with CTH/miR-21 NPs exhibited any apparent cytotoxicity compared with the unmodified Ti surface and polystyrene culture dishes ($p > 0.05$). The results were consistent with previous reports, and CTH/NPs showed potential as biocompatible, safe, and biodegradable vectors to deliver controlled-release miR-21.

The transfection efficiency was determined by flow cytometry after 24 hours of transfection (Figure 4D). FITC-labelled chitosan and Cy3-labelled miRNAs were employed to fabricate fluorescently labelled CTH/miR-21 NPs, and then these NPs were coated onto substrates according to a previous process. Generally, a higher loading concentration of CTH/miR-21 NPs induced higher transfection efficiencies with a dose-dependent pattern, which was in accordance with the results of the fluorescence microscopy. As shown in Figure 4D, the percentage of Cy3-positive cells increased significantly from 60% to nearly 85%, with the miR-21 concentration rising from 150 to 300 pmol/specimen. The miR-21 concentration of 300 pmol/specimen demonstrated comparable effects to the 450 pmol/specimen group. As such, we employed a 300 pmol/specimen concentration during the subsequent gingival fibroblast transfection.

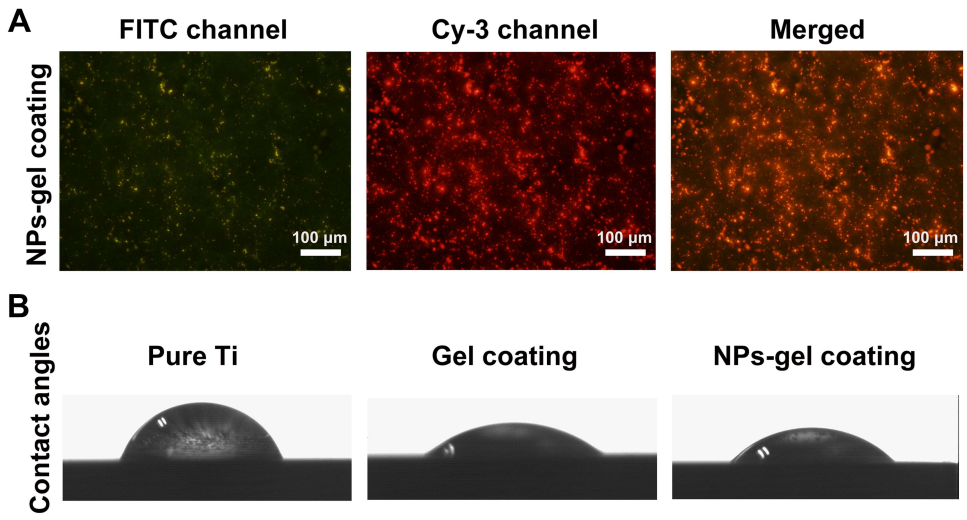

Figure 3 Fluorescence observation and water contact angle measurement of unmodified and coated Ti substrates.
Notes: (**A**) Fluorescence observation of CS/HA/miR-21 NP-coated Ti substrates. Fluorescein isothiocyanate (FITC)-labelled chitosan (green), Cy3-labelled miRNA-21 (red) and merged images. (**B**) The measurement of water contact angles on different substrates.

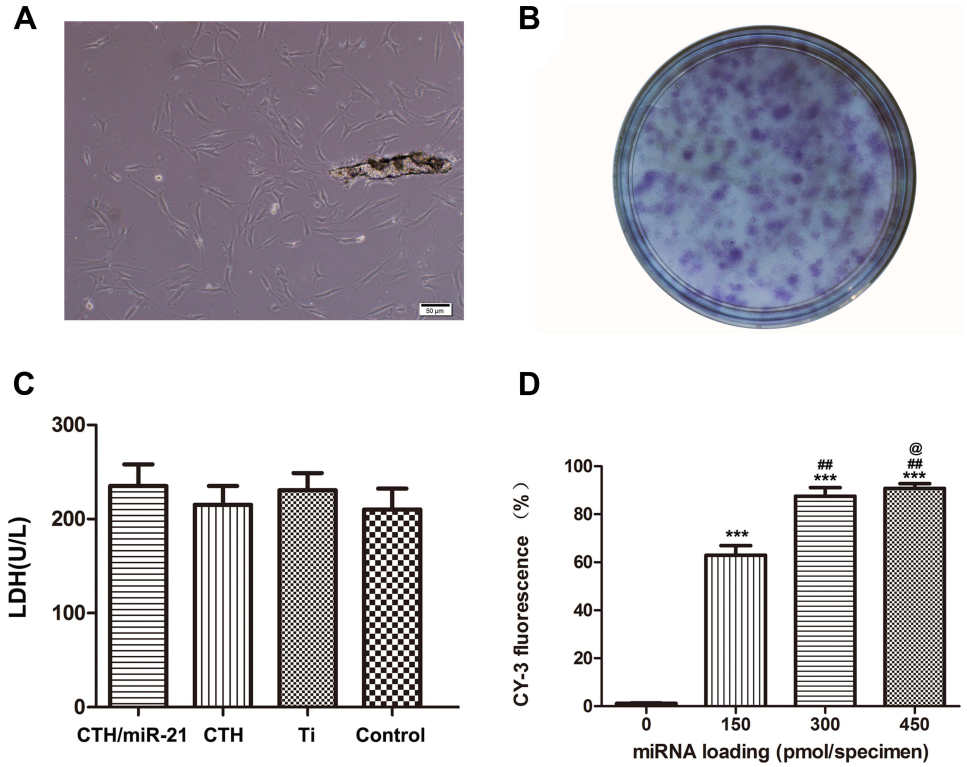

Figure 4 Transfection efficiency and cytotoxicity of the CTH/miR-21 NP-coated Ti substrates.
Notes: (**A**) Primary spindle-shaped fibroblasts grown in α-minimum essential medium (α-MEM) complete medium. (**B**) Images of the colony units formed by fibroblasts after 10 days of incubation. (**C**) Amount of LDH released by cells during the first 24 h after transfection. Control: polystyrene culture plate; Ti: smooth Ti substrates; CTH: vacant CTH NP-coated Ti substrates; CTH/miR-21: CTH/miR-21-coated Ti substrates. (**D**) Transfection efficiency. 150–450: CS/HA/miR-21 NP-coated Ti substrates at a concentration of 150–450 pmol/specimen miR-21. $^{***}p < 0.001$ vs the unmodified Ti surface; $^{\#\#}p < 0.01$ vs the 150 pmol/specimen miR-21 group; $^{@}p < 0.05$ vs the 300 pmol/specimen miR-21 group.

Fluorescence microscopy was employed to track internalized CTH/miR-21 NPs during the fibroblast culturing process on the CTH/miR-21 NP-coated Ti substrates after transfection for 1, 5, and 10 days. Figure 5 indicates that Cy3-labelled miR-21 and FITC-labelled CS accumulated near the nucleus inside the fibroblasts. The merged results showed

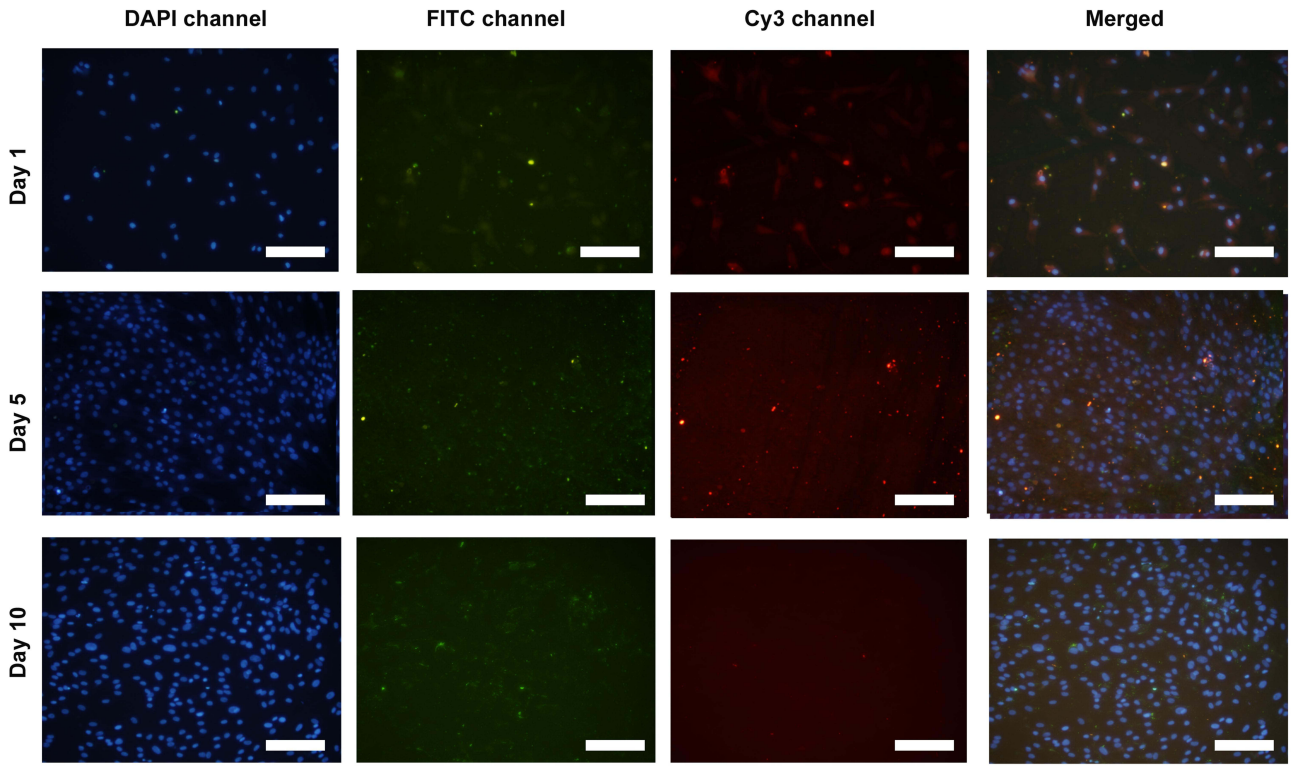

Figure 5 The tracks of fluorescently labelled CTH/miR-21 NPs after transfection for 1, 5, and 10 days.
Notes: Fluorescein 4', 6-diamidino-2-phenylindole (DAPI)-labelled nuclei (blue), isothiocyanate (FITC)-labelled chitosan (green), Cy3-labelled miRNA-21 s (red) and merged images. A concentration of 300 pmol/specimen miR-21 was used for reverse transfection.

enormous overlap between the Cy3 and FITC channels, indicating stable binding between CTH NPs and miR-21 during the observation time. However, with time, the fluorescence intensities of both Cy3-labelled miR-21 and FITC-labelled chitosan decreased gradually, especially that of Cy3-labelled miR-21. However, the fluorescence could still be observed after ten days, which implied a mild and slow-release transfection process during fibroblast incubation.

Cell Adhesion and Cell/Bacteria Proliferation Assay

DAPI staining and cell counting were used to measure the attached cell numbers on different substrates at 0, 0.25, 0.5, 1, and 2 hours after seeding. As Figure 6A shows, there were more fibroblasts adherent to gel-coated Ti substrates ($P < 0.01$) and NP-gel-coated Ti substrates ($P < 0.01$) than to polished Ti substrates during the entire observation period, and the differences in cell attachment were more significant at earlier time points (0.25 h and 0.5 h). Fibroblast proliferation was measured during a 5-day observation period using the CCK-8 assay. As shown in Figure 6B, cell growth on CTH/miR-21 NP-coated Ti specimens was significantly higher than that on vacant CTH/NP-coated and unmodified Ti substrates on days 1, 3 and 5 ($P < 0.05$). It seemed that slightly more fibroblasts grew on vacant CTH NP-coated Ti substrates than on highly polished Ti substrates on days 1 and 3, possibly because of the previously established excellent cell attachment to gel-CTH NP coating.[25] In addition, we also verified the influence of CTH/miR-21 NP-coated Ti specimens on the proliferation of Porphyromonas gingivalis, which is a gram-negative, anaerobic rod and considered to be among the major pathogens associated with adult periodontitis and Implantitis. The bacterial growth curve results (Figure S1) showed that there were no statistically significant differences in the proliferation of Porphyromonas gingivalis among the different samples.

Fibroblast Morphology

FE-SEM was employed to display the morphologies of cells grown on different substrates on day 5 when the cells and their extracellular secretions reached a state of maturity. As shown in Figure 7, slightly more cells grew on the CTH/miR-

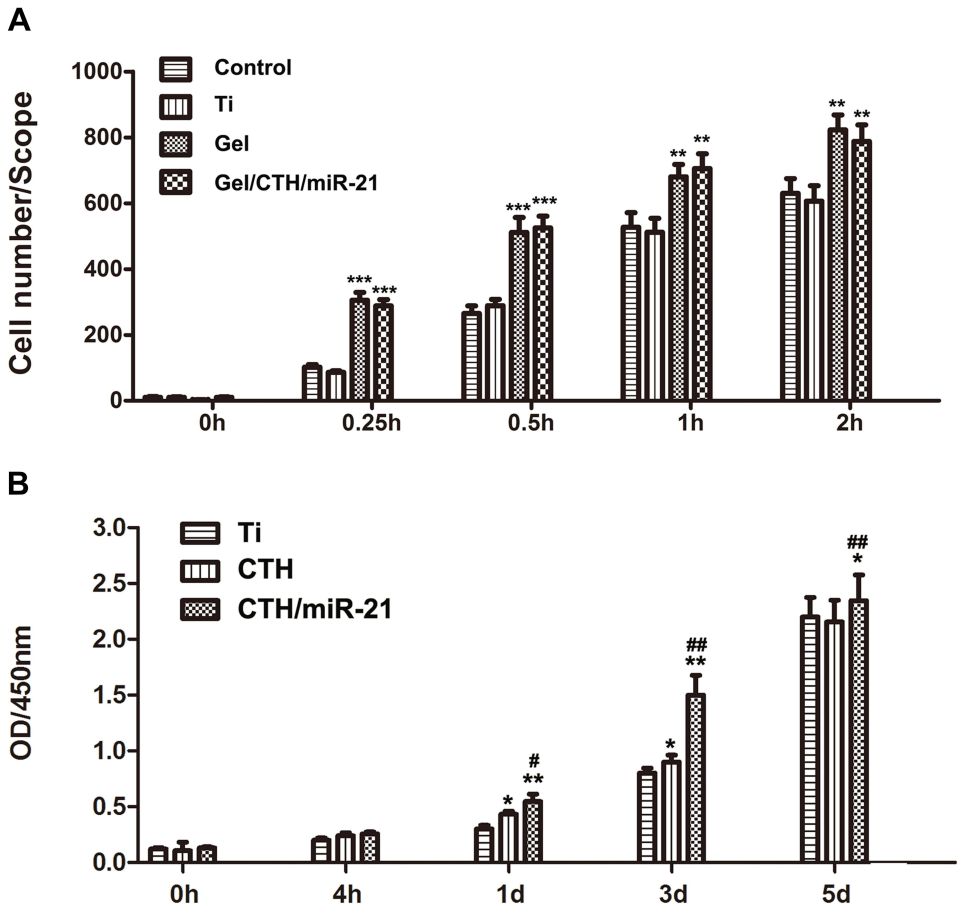

Figure 6 Cell adhesion and cell proliferation assay.
Notes: (**A**) Fibroblast adhesion on unmodified and coated Ti surface. (**B**) Fibroblast proliferation on unmodified and coated Ti surface. Control: polystyrene culture plate; Ti: unmodified smooth Ti substrates; Gel: gel-coated Ti substrates; CTH: vacant CTH NP-coated Ti substrates; CTH/miR-21: CTH/miR-21 NP-coated Ti substrates at a concentration of 300 pmol/specimen miR-21. Data are given as the mean ± SD, n = 6. (*, **, ***) $p < 0.05$, 0.01 and 0.001, respectively, vs the unmodified Ti substrates; $^{\#\#}p < 0.01$ and $^{\#}p < 0.5$ vs the vacant CTH NP-coated substrates.

21 NP-coated Ti substrates than on the noncoated smooth Ti substrates, and both types of Ti substrates presented very similar cell morphologies. The human gingival fibroblasts spread well on both miR-21-functionalised Ti substrates and smooth Ti surfaces with abundant filopodia and lamellipodia stretching out, anchoring themselves firmly onto the surface, and interweaving with each other.

ECM-Related Gene Expression

Real-time PCR was used to quantify the expression of the ECM-related genes COL1A1, COL3A1 and α-SMA on Ti substrates functionalized with miR-21 at concentrations of 150, 300 and 450 pmol/specimen, respectively, during seven days of incubation (Figure 8). Different samples generally induced different gene expression levels in a dose- and time-dependent manner. After three days of reverse transfection, the 150, 300 and 450 pmol samples all showed higher expression levels of COL1A1 and COL3A1 compared to the control group, while both the 150 and 300 pmol groups showed similar expression of α-SMA to smooth Ti specimens except for the 450 pmol group. The 450 pmol group had the highest expression levels of the three genes among all groups. On day 7, the 150, 300, and 450 pmol/specimen groups all exhibited upregulated expression of COL1A1, COL3A1 and α-SMA to varying degrees compared with that obtained in the smooth Ti specimens, while the 300 pmol miR-21 group induced the highest expression (≈ 8.2-fold) of α-SMA on day 7 ($P < 0.01$). The above results indicated that the application of CTH/miR-21 NPs can effectively upregulate the in vitro expression of ECM-related genes.

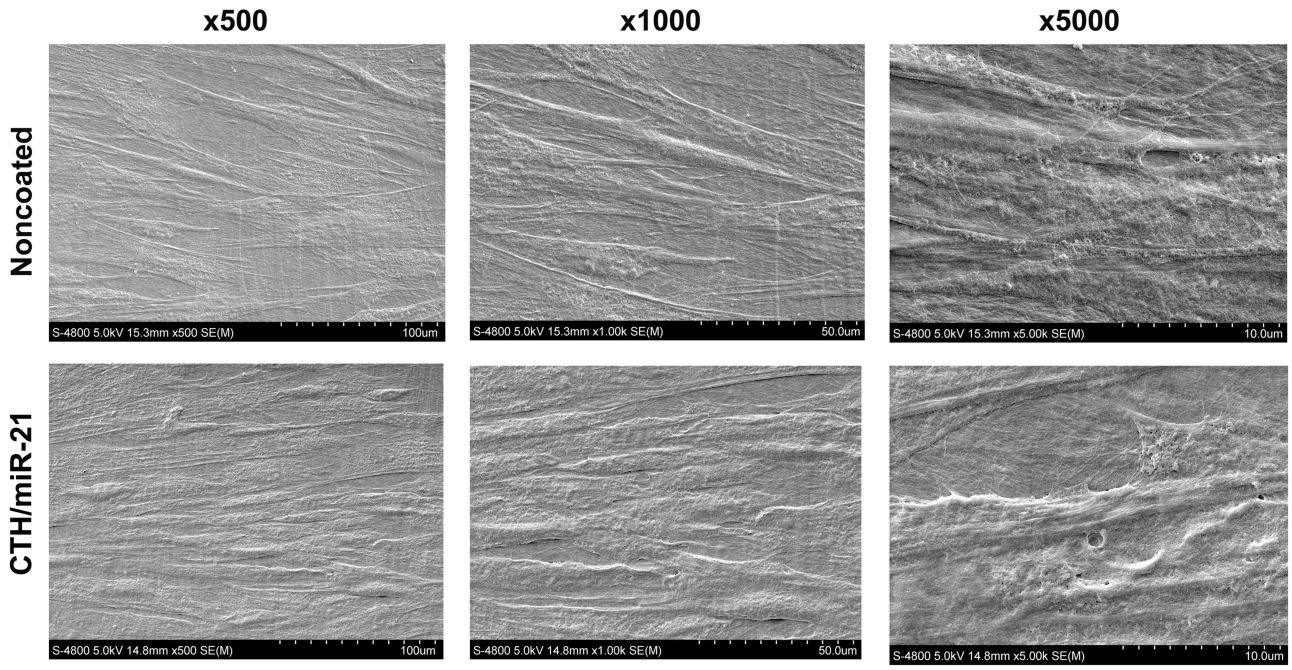

Figure 7 SEM images showing the cell morphology after five days of incubation on noncoated and CTH/miR-21 NP-coated smooth Ti substrates.
Notes: Noncoated: noncoated smooth Ti substrates; CTH/miR-21: CTH/miR-21 NP-coated Ti substrates at a concentration of 300 pmol/specimen miR-21.

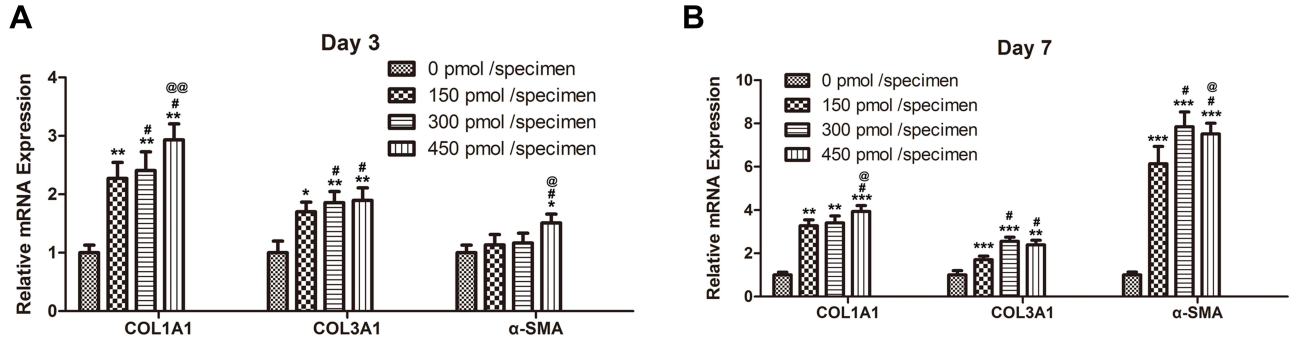

Figure 8 Relative gene expression levels of COL1A1, COL3A1 and α-SMA on different substrates.
Notes: Fibroblasts were cultured on CS/HA/miR-21 NP-coated Ti substrates at a concentration of 150–450 pmol/specimen miR-21 on days 3 (**A**), and 7 (**B**). All values were normalized to GAPDH. (*, **, ***) $p < 0.05$, 0.01 and 0.001, respectively, vs unmodified Ti substrates; $^{\#}p < 0.05$ vs 150 pmol/specimen miR-21 group; $^{(@.\ @@)}$ $p < 0.05$ and 0.01 vs 300 pmol/specimen miR-21 group.

Discussion

The formation of an enhanced biological seal at percutaneous areas of implants is a key clinical issue. In this design, CS/TPP/HA/miR-21 (CTH/miR-21) nanoparticles were designed, characterized, and cross-linked onto smooth Ti substrates with 0.2% gel solution for reverse transfection. Afterwards, isolated human gingival fibroblasts were seeded on the functionalized Ti surface. Furthermore, we evaluated the transfection efficiency, cytotoxicity, adhesion, and ECM-related gene expression in human gingival fibroblasts.

CTH nanoparticles were produced via ionic gelation between positively charged CS and negatively charged HA and TPP. According to our previous works,[26] with an increasing amount of HA, the particle size significantly increased from ~146.0 nm to ~277.7 nm, while the zeta potential dropped from +43.5 to +21.5 mV. At the same time, the incorporation of miR-21 at an N/P ratio of 20:1 did not change the particle size or surface charge.[21] The binding capacity of miR-21 with CTH nanoparticles was confirmed by gel retardation measurements. The results demonstrated

that miR-21 remained completely within the agarose gel loading well when the N/P ratio exceeded 15:1, which was consistent with our previous reports. Compared with pDNA, miRNA presented a less negative charge with a shorter molecular chain, which was difficult to combine with CS at a low N/P ratio. Therefore, it was necessary to increase the N/P ratios to improve the loading efficiency of miR-21. However, other researchers found that higher N/P ratios could lead to a larger excess of free chitosan and increase the chance of ineffective interactions on cell surfaces.[26] Wu et al[21] and Ping et al[27] fabricated CS/miRNA or siRNA nanoparticles at an N/P ratio of 20 and reached maximum knockdown efficiency. Therefore, we fabricated CTH miR-21 NPs with a CS:TPP:HA ratio of 1:0.15:0.1 and an N/P ratio of 20:1 for this study.

Previous studies have indicated that appropriate topography of percutaneous Ti surfaces tends to enhance the biological effects of fibroblasts, including cell adhesion, cell proliferation, ECM deposition and so on. Previous studies have shown that rougher Ti substrates with more ridges and troughs present physical barriers to the attachment and spreading of cells, subsequently leading to a decrease in cell accumulation.[28] Smooth-polished Ti surfaces have been widely used as percutaneous parts of implants. To improve the quantity and quality of newly formed fibrous tissue and form a stable biological seal around percutaneous areas in the early stage, CTH/miR-21 NP-coated smooth Ti surfaces were designed, and miR-21 was delivered into the involved dermal fibroblasts as a posttranscriptional regulator. After endocytosis and degradation of CTH/miR-21 NPs, enhanced fibrous tissue could still be formed on the revealable smooth Ti surface.

The above results indicated high transfection efficiency due to reverse transfection.[29] In this work, CTH/miR-21 NPs were preplated onto Ti substrates; therefore, these NPs could directly reach the adherent fibroblasts and be incorporated into the cells, in contrast to the usual delivery of a large amount of free transfection reagents in the medium. This kind of substrate-mediated transfection may facilitate endocytosis by three mechanisms:[20] first, the relatively high zeta potential (34.2 ± 5.3) of CTH/miR-21 NPs, mainly contributed by CS, tends to induce close contact with cell membranes with a negative charge; second, the specific binding between HA and CD44 receptors of human gingival fibroblasts facilitates the internalization process; and third, HA can promote the endocellular release of miR-21 from the complexes by weakening the tight binding between miR-21 and the vectors near the perinuclear region, leading to faster nucleic acid release[21] and thus favouring specific gene expression. The results were consistent with previous research on reverse transfection with miRNA[20] and siRNA.[27]

As a kind of anchorage-dependent cell, fibroblasts need to form a suitable attachment to a substrate early to provide signals required for normal biological activities; otherwise, apoptosis will occur.[30] Gel has been widely used as a mediator to promote enhanced cell adhesion on a variety of coated surfaces due to its favourable cytocompatibility and hydrophilic performance in previous studies.[31] Chitosan-based NPs can also interact with the phosphatide groups of the cytomembrane through hydrophobic and electrostatic interactions, which may contribute to the appropriate adhesive capability and cell permeability. We did not find any apparent differences ($P > 0.05$) in adhesive capacity between the gel-coated Ti surface and the NPs-gel-coated Ti surface at the indicated time, which implies that the gel may be primarily responsible for the cell attachment of this composite in this design.

This result indicated that the internalization of miR-21 may contribute to the faster growth of fibroblasts. Previous researchers also reported that the increased miR-21 could promote the proliferation potential of fibroblasts in the development and progression of skin fibrosis, such as hypertrophic scars, keloids, and sclerodermas, and was accountable for the rapid growth of skin fibrosis.[32] Jafarinejad-Farsangi et al[33,34] revealed that miR-21 could promote fibroblast proliferation and decrease the rate of apoptosis. The underlying mechanism of this stimulatory effect may be that miR-21 could downregulate PTEN expression and influence fibroblast proliferation and apoptosis through the AKT signalling pathway according to previous reports, and the miR-21/PTEN/AK signalling pathway may play essential roles in fibroblast proliferation.[33]

According to Jafarinejad-Farsangi's reports, the skin lesions and fibroblasts always exhibit high expression levels of miR-21 as a profibrotic factor.[34] Zhou et al[35] found that miR-21 could stimulate collagen deposition in keloids by downregulating SMAD7 in fibroblasts. They also reported that miR-21 mimics could negatively regulate the expression of SMAD7 to increase the expression of Col1A1 and Col3A1. The miR-21/SMAD7 pathway may regulate collagen I and III synthesis in keloid-derived fibroblasts by mediating p38 phosphorylation.[36] α-SMA is the actin isoform that

predominates within myofibroblasts and plays a vital role in developing the fibrotic response.[37] According to previous reports,[17,38] miR-21 was responsible for fibroblast differentiation into myofibroblasts, a form of fibroblast cells characterized by the upregulated expression of α-SMA with enhanced capacity to migrate and the production of ECM.[39] Once activated, myofibroblasts stop proliferating and produce large amounts of extracellular proteins.[5] The present in vitro study verified the feasibility of designing a CTH/miR-21 NP coating on smooth Ti substrates and showed the use of miR-21 with high transfection efficiency of to adjust the biological functions of gingival fibroblasts. We also plan to investigate the in vivo effects of this miR-21 delivery approach, including the production of extracellular matrix and the bonding strength of skin-implant biointegration at percutaneous parts.

Conclusions

In this study, we aim to develop a compact biological seal between the gingiva and the implant interface by means of miR-21 delivery to the human gingival fibroblasts around the percutaneous parts of the implant. First, we designed CS/TPP/HA nanoparticles with an optimal CS:TPP:HA ratio (1:0.15:0.1) and N/P ratio (20:1) as vectors to load miR-21. Subsequently, we cross-linked CTH/miR-21 NPs onto smooth Ti substrates through 0.2% gel solution for reverse transfection. Afterwards, the isolated gingival fibroblasts were incubated on CTH/miR-21 NP-coated Ti substrates. The miR-21-functionalized smooth Ti surfaces exhibited analogous cytotoxicity and cell morphologies to those of cells on the smooth Ti substrates and had increased cell adhesion ($P < 0.01$), enhanced cell proliferation ($P < 0.05$) and upregulated ECM-related gene expression. This work suggests that chitosan-based NPs may be an efficient nonviral miR-21 vector for the formation of early tight skin-implant biointegration when designing percutaneous implants.

Abbreviations

miR-21, microRNA-21; CS, chitosan; TPP, tripolyphosphate; HA, hyaluronic acid; NPs, nanoparticles; CTH NPs, chitosan/tripolyphosphate/hyaluronic acid nanoparticles; N/P ratio, the molar ratio of the positive CS amino group versus the negative miRNA phosphate group; ECM, extracellular matrix; α-SMA, alpha-smooth muscle action; UTR, untranslated region; CFU-F, colony-forming unit-fibroblast; LDH, lactate dehydrogenase; COL1A1, collagen type Iα1; COL3A1, collagen type IIIα1; MSCs, mesenchymal Stem Cell; FITC, fluorescein isothiocyanate; Cy3, Cyanine 3; pDNA, plasmid DNA; siRNA, small interfering RNA.

Acknowledgments

This research was supported by the National Natural Science Foundation of China (Project No.: 81700930) and the Shaanxi Science and Technology Research and Development Project (Project No.: 2021SF-105). The authors appreciate the Department of Biopharmaceuticals, School of Pharmacy, Air Force Medical University.

Disclosure

The authors report no conflicts of interest in this work.

References

1. Gomez-Vega JM, Saiz E, Tomsia AP. Glass-based coatings for titanium implant alloys. *J Biomed Mater Res*. 1999;46(4):549–559. doi:10.1002/(SICI)1097-4636(19990915)46:4<549::AID-JBM13>3.0.CO;2-M
2. Wang Z, Wu G, Bai S, et al. MAPs/bFGF-PLGA microsphere composite-coated titanium surfaces promote increased adhesion and proliferation of fibroblasts. *Biomed Mater*. 2014;9(3):035006. doi:10.1088/1748-6041/9/3/035006
3. Pendegrass CJ, Lancashire HT, Fontaine C, Chan G, Hosseini P, Blunn GW. Intraosseous transcutaneous amputation prostheses versus dental implants: a comparison between keratinocyte and gingival epithelial cell adhesion in vitro. *Eur Cell Mater*. 2015;29:237–249. doi:10.22203/eCM.v029a18
4. Liu Y, Li Y, Li N, et al. TGF-β1 promotes scar fibroblasts proliferation and transdifferentiation via up-regulating MicroRNA-21. *Sci Rep*. 2016;6(1):32231. doi:10.1038/srep32231
5. Shinde AV, Humeres C, Frangogiannis NG. The role of α-smooth muscle actin in fibroblast-mediated matrix contraction and remodeling. *Biochim Biophys Acta Mol Basis Dis*. 2017;1863(1):298–309. doi:10.1016/j.bbadis.2016.11.006
6. Chung Y, Fu E, Chin YT, et al. Role of Shh and TGF in cyclosporine-enhanced expression of collagen and α-SMA by gingival fibroblast. *J Clin Periodontol*. 2015;42(1):29–36. doi:10.1111/jcpe.12333

7. Chimutengwende-Gordon M, Pendegrass C, Blunn G. The in vivo effect of a porous titanium alloy flange with hydroxyapatite, silver and fibronectin coatings on soft-tissue integration of intraosseous transcutaneous amputation prostheses. *Bone Joint J*. 2017;99(3):393–400. doi:10.1302/0301-620X.99B3.BJJ-2016-0360.R1
8. Hansen SK, Rainey PB, Haagensen JA, Molin S. Evolution of species interactions in a biofilm community. *Nature*. 2007;445(7127):533–536. doi:10.1038/nature05514
9. Chowdhury M, Ntiribinyange M, Nyamayaro K, Fester V. Photocatalytic activities of ultra-small β-FeOOH and TiO2 heterojunction structure under simulated solar irradiation. *Mater Res Bull*. 2015;68:133–141. doi:10.1016/j.materresbull.2015.03.044
10. Li K, Xue Y, Yan T, Zhang L, Han Y. Si substituted hydroxyapatite nanorods on Ti for percutaneous implants. *Bioact Mater*. 2020;5(1):116–123. doi:10.1016/j.bioactmat.2020.01.001
11. Wang X, Lei X, Yu Y, et al. Biological sealing and integration of a fibrinogen-modified titanium alloy with soft and hard tissues in a rat model. *Biomater Sci*. 2021;9(15):5192–5208. doi:10.1039/D1BM00762A
12. Deshmukh S, Sternberg K, Hernandez N, Eisner BH. Compliance with American urological association guidelines for post-percutaneous nephrolithotomy antibiotics does not appear to increase rates of infection. *J Urol*. 2015;194(4):992–996. doi:10.1016/j.juro.2015.04.097
13. Renvert S, Polyzois I, Claffey N. How do implant surface characteristics influence peri-implant disease? *J Clin Periodontol*. 2011;38(Suppl 11):214–222. doi:10.1111/j.1600-051X.2010.01661.x
14. Bartel DP. MicroRNAs: genomics, biogenesis, mechanism, and function. *Cell*. 2004;116(2):281–297. doi:10.1016/S0092-8674(04)00045-5
15. Cheng C, Zhang Z, Wang S, Chen L, Liu Q. Reduction sensitive CC9-PEG-SSBPEI/miR-148b nanoparticles: synthesis, characterization, targeting delivery and application for anti-metastasis. *Colloids Surf B Biointerfaces*. 2019;183:110412. doi:10.1016/j.colsurfb.2019.110412
16. Tao H, Zhang JG, Qin RH, et al. LncRNA GAS5 controls cardiac fibroblast activation and fibrosis by targeting miR-21 via PTEN/MMP-2 signaling pathway. *Toxicology*. 2017;386:11–18. doi:10.1016/j.tox.2017.05.007
17. Xu H, Ling M, Xue J, et al. Exosomal microRNA-21 derived from bronchial epithelial cells is involved in aberrant epithelium-fibroblast cross-talk in COPD induced by cigarette smoking. *Theranostics*. 2018;8(19):5419–5433. doi:10.7150/thno.27876
18. Lu KC, Wu CC, Yen JF, Liu WC. Vascular calcification and renal bone disorders. *ScientificWorldJournal*. 2014;2014:637065. doi:10.1155/2014/637065
19. Luo M, Tan X, Mu L, et al. MiRNA-21 mediates the antiangiogenic activity of metformin through targeting PTEN and SMAD7 expression and PI3K/AKT pathway. *Sci Rep*. 2017;7(1):43427. doi:10.1038/srep43427
20. Wang Z, Wu G, Feng Z, et al. Microarc-oxidized titanium surfaces functionalized with microRNA-21-loaded chitosan/hyaluronic acid nanoparticles promote the osteogenic differentiation of human bone marrow mesenchymal stem cells. *Int J Nanomedicine*. 2015;10:6675–6687. doi:10.2147/IJN.S94689
21. Wu G, Feng C, Quan J, et al. In situ controlled release of stromal cell-derived factor-1α and antimiR-138 for on-demand cranial bone regeneration. *Carbohydr Polym*. 2018;182:215–224. doi:10.1016/j.carbpol.2017.10.090
22. Liu M, Zhang Y, Wu C, Xiong S, Zhou C. Chitosan/halloysite nanotubes bionanocomposites: structure, mechanical properties and biocompatibility. *Int J Biol Macromol*. 2012;51(4):566–575. doi:10.1016/j.ijbiomac.2012.06.022
23. Hang C, Zou Y, Zhong Y, Zhong Z, Meng F. NIR and UV-responsive degradable hyaluronic acid nanogels for CD44-targeted and remotely triggered intracellular doxorubicin delivery. *Colloids Surf B Biointerfaces*. 2017;158:547–555. doi:10.1016/j.colsurfb.2017.07.041
24. Sacco P, Paoletti S, Cok M, et al. Insight into the ionotropic gelation of chitosan using tripolyphosphate and pyrophosphate as cross-linkers. *Int J Biol Macromol*. 2016;92:476–483. doi:10.1016/j.ijbiomac.2016.07.056
25. Fraioli R, Rechenmacher F, Neubauer S, et al. Mimicking bone extracellular matrix: integrin-binding peptidomimetics enhance osteoblast-like cells adhesion, proliferation, and differentiation on titanium. *Colloids Surf B Biointerfaces*. 2015;128:191–200. doi:10.1016/j.colsurfb.2014.12.057
26. Wu G, Feng C, Hui G, et al. Improving the osteogenesis of rat mesenchymal stem cells by chitosan-based-microRNA nanoparticles. *Carbohydr Polym*. 2016;138:49–58. doi:10.1016/j.carbpol.2015.11.044
27. Ping Y, Liu C, Zhang Z, Liu KL, Chen J, Li J. Chitosan-graft-(PEI-β-cyclodextrin) copolymers and their supramolecular PEGylation for DNA and siRNA delivery. *Biomaterials*. 2011;32(32):8328–8341. doi:10.1016/j.biomaterials.2011.07.038
28. Scarano A, Piattelli A, Polimeni A, Di Iorio D, Carinci F. Bacterial adhesion on commercially pure titanium and anatase-coated titanium healing screws: an in vivo human study. *J Periodontol*. 2010;81(10):1466–1471. doi:10.1902/jop.2010.100061
29. He CX, Li N, Hu YL, et al. Effective gene delivery to mesenchymal stem cells based on the reverse transfection and three-dimensional cell culture system. *Pharm Res*. 2011;28(7):1577–1590. doi:10.1007/s11095-011-0390-0
30. Ayuk SM, Abrahamse H, Houreld NN. The role of photobiomodulation on gene expression of cell adhesion molecules in diabetic wounded fibroblasts in vitro. *J Photochem Photobiol B*. 2016;161:368–374. doi:10.1016/j.jphotobiol.2016.05.027
31. Narita T, Hirai A, Xu J, Gong JP, Osada Y. Substrate effects of gel surfaces on cell adhesion and disruption. *Biomacromolecules*. 2000;1(2):162–167. doi:10.1021/bm9900085
32. Li Y, Zhang J, Lei Y, Lyu L, Zuo R, Chen T. MicroRNA-21 in skin fibrosis: potential for diagnosis and treatment. *Mol Diagn Ther*. 2017;21(6):633–642. doi:10.1007/s40291-017-0294-8
33. Liu Y, Wang X, Yang D, Xiao Z, Chen X. MicroRNA-21 affects proliferation and apoptosis by regulating expression of PTEN in human keloid fibroblasts. *Plast Reconstr Surg*. 2014;134(4):561e–573e. doi:10.1097/PRS.0000000000000577
34. Jafarinejad-Farsangi S, Gharibdoost F, Farazmand A, et al. MicroRNA-21 and microRNA-29a modulate the expression of collagen in dermal fibroblasts of patients with systemic sclerosis. *Autoimmunity*. 2019;52(3):108–116. doi:10.1080/08916934.2019.1621856
35. Zhou R, Wang C, Wen C, Wang D. miR-21 promotes collagen production in keloid via Smad7. *Burns*. 2017;43(3):555–561. doi:10.1016/j.burns.2016.09.013
36. Li J, Zhao L, He X, Yang T, Yang K. MiR-21 inhibits c-Ski signaling to promote the proliferation of rat vascular smooth muscle cells. *Cell Signal*. 2014;26(4):724–729. doi:10.1016/j.cellsig.2013.12.013
37. Kawasaki Y, Imaizumi T, Matsuura H, et al. Renal expression of alpha-smooth muscle actin and c-Met in children with Henoch-Schönlein purpura nephritis. *Pediatr Nephrol*. 2008;23(6):913–919. doi:10.1007/s00467-008-0749-6
38. Kilari S, Cai C, Zhao C, et al. The role of MicroRNA-21 in venous neointimal hyperplasia: implications for targeting miR-21 for VNH treatment. *Mol Ther*. 2019;27(9):1681–1693. doi:10.1016/j.ymthe.2019.06.011
39. Elberg G, Chen L, Elberg D, Chan MD, Logan CJ, Turman MA. MKL1 mediates TGF-beta1-induced alpha-smooth muscle actin expression in human renal epithelial cells. *Am J Physiol Renal Physiol*. 2008;294(5):F1116–F1128. doi:10.1152/ajprenal.00142.2007